Characterization of Rhodamine 6G Aggregates Intercalated in Solid Thin Films of Laponite Clay. 1. Absorption Spectroscopy

V. Martínez Martínez, F. López Arbeloa,* J. Bañuelos Prieto, T. Arbeloa López, and I. López Arbeloa

Departamento de Química Física, Universidad del País Vasco-EHU, Apartado 644, 48080 Bilbao, Spain

Received: June 7, 2004; In Final Form: October 13, 2004

The aggregation process of Rhodamine 6G (R6G) laser dye intercalated in supported thin films of Laponite clay (Lap) is analyzed by means of electronic absorption spectroscopy. Two procedures are proposed to express the analytical dye concentration of the solid samples with respect to a reference-diluted dye film by means of a normalization-concentration factor. From the evolution of the concentration-normalized absorption spectra with the concentration factor, analyzed by means of a nonlinear least-squares fitting equation obtained from the mass law, the absorption characteristics and the aggregation constant of the dimer of R6G in Lap films were evaluated in moderate dye/clay loadings (1−25% of the total cation exchangeable capacity, CEC, of Lap clay). An oblique head-to-tail dimer was characterized by applying the exciton theory with an intermonomeric distance of around 9.5 Å and a torsion angle between the long molecular axis units of around 105°. This dimer contrasts with the twisted sandwich-type dimer of R6G previously observed in Lap particles in aqueous suspensions, probably because the limitation of the interlayer space in solid samples does not allow sandwich-type aggregates with a parallel disposition of the aromatic ring into the clay surface. A higher-order aggregate of R6G is observed in high loading samples (>25% CEC).

Introduction

The incorporation of photofunctional dye molecules into inorganic solid systems is of great technological interest for the design of photonic devices with potential applications as solid tunable lasers, antenna systems, optical switches, sensors, etc.[1−9] Indeed, the adsorption of dyes into solid host systems can ameliorate the photophysical properties of the dye, and the host matrix can act as a protection for thermal decompositions and photobleaching of the dye, improving the operation and lifetime of the dye as photonic materials. Besides, host/guest assemblies can build up high-organized inorganic−organic nanostructures. The inorganic material provides a template for the guest molecules, and depending on several dye−dye and dye−host interactions, the dye molecules could be intercalated with a preferential orientation.[10−28] In this sense, Rhodamine 6G (R6G) cationic dye is one of the most interesting and useful laser dyes to be incorporated in solid host materials.[29]

Clay layered materials are adequate inorganic systems to accommodate organocationic molecules due to their cationic exchange capacity (CEC, up to 4 negative charges per cell unit) and high area/weight ratio (up to 1000 m^2/g).[30−33] Clay layers can be stacked in a parallel arrangement, giving rise to the interlayer space, characterized by a nanoscale distance. Moreover, clays are mineral materials, and their natural abundance and low cost make them an interesting host for cationic dyes. In this sense, smectite type clays, with a moderate cation exchange capacity (CEC around 0.5−1.2 negative charge per cell unit), have been widely used as host materials owing to the swelling characteristics of their interlayer spaces, which can incorporate a multitude of cationic and polar organic molecules. Transparent films of these inorganic solids would be one of the best ways to manufacture macroscopic multilayered structures with 2D well-ordered host assemblies for cationic dyes. Taking into account that the interlayer space of stacked clay particles is around 13 Å, ordered clay films will provide a nanostructured confined space in a macroscopic bidimensional array for organic molecules.

Previously, the incorporation of R6G molecules into the interlayer space of supported Laponite (Lap) clay films[34] was characterized by several techniques. Atomic force and scanning electron microscopy images confirmed that Lap films obtained by spin-coating technique showed an adequate and parallel distribution of the clay particles overall the support plate. The incorporation of the dye into the interlayer space was confirmed by X-ray diffraction data, whereas absorption and fluorescence spectra suggested the aggregation of the dye at the clay surfaces. In this paper, the dimerization constant of R6G in Lap thin film is evaluated, and the geometry of the aggregate present in the interlayer space of Lap films is analyzed.

The molecular aggregation can drastically modify the absorption characteristics (spectral shifts and band splitting) of the dye by increasing the dye concentration.[35−37] Moreover, the fluorescence quantum yield and decay time could also be significantly decreased by the associative process.[38,39] The first stage of the dye aggregation, for example in moderate dye concentrations, should be the formation of the dimer, but further increases in the dye concentration would lead to the formation of high-order aggregates. The exciton theory,[40,41] a quantum mechanic method considering the electrostatic interactions between the dipole moment of monomeric units, can be applied to interpret these spectral changes. It predicts a different electronic energy diagram and photophysical behavior of the dimer depending on the geometric distribution of the monomer units in the aggregate.

* Corresponding author: phone +34 94 601 59 71; fax +34 94 464 85 00; e-mail qfploarf@lg.ehu.es.

10.1021/jp047552e CCC: $27.50
Published on Web 11/25/2004

SCHEME 1: Exciton Splitting of the Electronic States for Different Geometric Dispositions of the Monomer Units in the Dimer

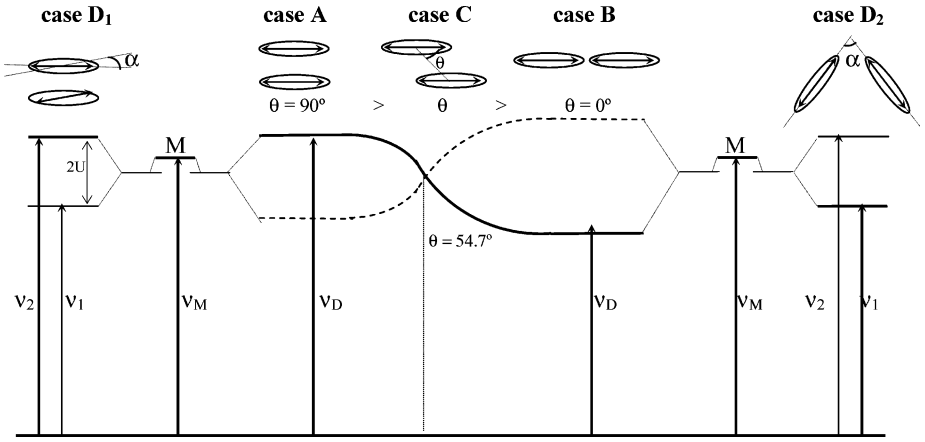

This theory suggests a two-excited states splitting of the monomer electronic transition for the dimer. The energy gaps and the transition probabilities from the ground to these excited states depend on the relative orientation of the transition moment vector of the monomeric units in the aggregate. Taking into account the angle between the direction of the dipolar moments and the line linking the molecular centers (θ) and the angle between the transition moments of the monomers in the dimer (α), several specific cases can be considered (Scheme 1).

Case A: Perfect Sandwich Dimer (H-Dimer). The dipole moments of the monomeric units are aligned and in parallel planes ($\theta = 90°$ and $\alpha = 0°$). The spectroscopic transition from the ground state to the most energetic excited state is an allowed transition (equal to 2*f*, for example twice the oscillator strength of the monomer transition, *f*), while the transition to the lowest energetic excited state is forbidden (the subtraction vector becomes zero). As a result, the absorption spectrum of the dimer would consist of an absorption band placed at higher energies with respect to the monomer band (the so-called H-band). The aggregate becomes a nonfluorescent species (fast nonradiative deactivation to the lowest excited state which is not fluorescent), but it can be a potential quencher of the fluorescence of the monomeric units due to the enhancement of the deactivation via the triplet state.[41]

Case B: In-Line Head-to-Tail Dimer (J-Dimer). The dipole moments are coplanar and in-line ($\theta = 0°$ and $\alpha = 0°$). This is the opposite case to the H-dimer; the spectroscopically allowed transition (with an oscillator strength of 2*f*) is now the energy gap between the ground and the lowest excited state, and the dimer can fluoresce.[41] In this case, a bathochromic band (J-band) with respect to the monomer band would be observed in both the absorption and fluorescence spectra.

Cases A and B are extreme and idealistic geometries, and in general the aggregate can adopt structures with intermediate θ and α angles. Indeed, the geometry of the dimer should be that in which the monomeric units are oriented in such a way as to optimize the attractive permanent/induced/instantaneous dipole interactions and to minimize the repulsive interactions and steric hindrances between monomeric units in the aggregate.[35−37,42]

Case C: Coplanar ($\alpha = 0°$) Displaced Dimer ($0° < \theta < 90°$). In this case, the dimer would present an absorption band placed at higher/lower energies with respect to that of the monomer band for θ angles lower/higher than 54.7°. For dimers with $\theta < 54.7°$, the so-called J-sandwich dimers, the aggregate should be fluorescent. For an angle $\theta = 54.7°$ there will be no effects in the splitting.

Case D. Both H- and J-bands will be observed in the absorption spectra for a twisted sandwich dimer ($\theta = 90°$ and α any value, case D_1 in Scheme 1) or for an oblique head-to-tail dimer ($\theta = 0°$ and α any value, case D_2). The H-band will be more intense for the sandwich dimer, whereas a head-to-tail dimer is achieved if the J-band is more intense. Fujii et al.[43] have proposed the ratio between the absorption intensities (obtained from the area under the curve) of both H- and J-bands as an indicative parameter for the type of dimer: thus, values of $A_H/A_J \geq 1.3$ and ≤ 0.7 are indicative of a sandwich and a head-to-tail geometry, respectively.

Although some of these aggregates can theoretically emit, their relative quantum yield would be much smaller than that of the monomer.[44]

The aggregation process of rhodamine dyes has been extensively studied by spectroscopic methods both in solutions[35−37] and in clay suspension.[45−50] The tendency of rhodamine dyes to aggregate strongly depends on the hydrophobicity of the environment and the limitation of the interlayer space of the clays, among other factors. Thus, twisted sandwich and oblique head-to-tail dimers, trimers, and even higher order aggregates of rhodamine dyes have been found in several media.

In this paper, the dimer of R6G adsorbed in the interlayer space of solid Lap films is spectroscopically characterized by absorption spectroscopy. R6G is a cationic dye and probably the most commonly used laser dye,[29] whereas Lap clay is a very pure synthetic smectite[51] providing optimal transparency films to the visible radiation due to the small particle size. This paper describes the manipulation of the recorded absorption spectra of the dye in order to normalize the dye concentration of the solid samples to a common diluted R6G loading Lap film sample used as reference. Different mathematical procedures are adapted to evaluate the absorption characteristic and the association constant of the dimer of R6G in a solid system such as the present supported thin films of Lap clay. The fluorescent behavior of the R6G aggregates in Lap supported films will be discussed in a second paper.[52]

Experimental Section

Rhodamine 6G (laser grade), R6G, was supplied by Kodak and was used without further purification. Two R6G solutions were prepared: 10^{-5} and 10^{-3} M in water (Milli-Q)/ethanol mixture with a water molar fraction of $x_w = 0.8$. This mixture was previously checked to be the most adequate to get homogeneous distribution of the adsorbed dye molecules into the interlayer space of Lap films.[34]

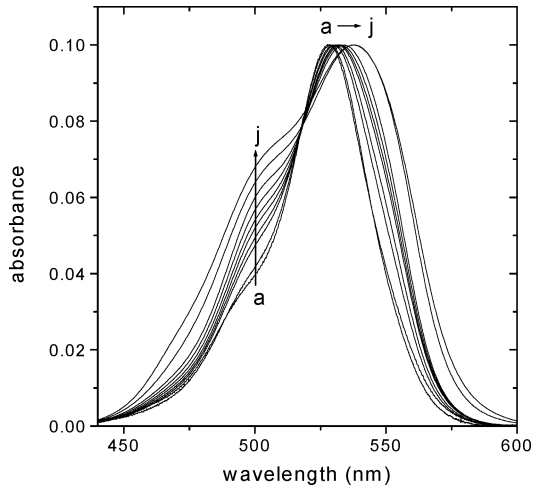

Figure 1. Height-normalized absorption spectra of R6G adsorbed in Lap films for different relative dye/clay concentrations (in % CEC): 0.1 (a), 1.0 (b), 2.0 (c), 3.2 (d), 5.7 (e), 10 (f), 14 (g), 21 (h), 45 (i), and 60 (j).

Synthetic Laponite (Lap) clay with a cationic exchange capacity (CEC) of 77.3 mequiv/100 g was supplied by Laporte Industries Ltd. and was used as received. Some drops of a 20 g L^{-1} clay aqueous suspension were distributed on a glass plate, and supported thin films were obtained by the spin-coating technique (BLE spinner, model Delta 10). The thickness of the film can be controlled from the viscosity of clay solutions, the speed rate of the spin-coating procedure, and the number of spinnings. In the present case, atomic force microscopy reveals Lap thickness films around 450 nm at the center of the support plate for double-coverage procedures at 2500 rpm spin speed for 60 s.[34] This thickness was checked to be identical for all samples prepared in the same spinning conditions. Transparent and crackless Lap films (checked by scanning electron microscopy images[34]) were obtained by this technique. R6G dye was incorporated into Lap films by immersion of the film in a R6G solution at room temperature. The loading of the dye was controlled by the concentration of the dye solution (10^{-3} and 10^{-5} M) and the immersion time (from a few minutes up to 2 days). After the adsorption of the dye in the films, the samples were rinsed in ethanol and water to eliminate external species and finally were dried overnight in an airflow oven at 35 °C. The X-ray diffraction technique was used to confirm the incorporation of dye molecules in the interlayer space.[34]

The vis absorption spectra of R6G/Lap films were recorded on a double-beam Varian spectrophotometer (model CARY 4E) by the transmittance method with a scan speed of 60 nm/min and 1 nm bandwidth incident light. The absorption spectra of R6G/Lap were corrected from the signal of the Lap by placing a Lap film (without dye) in the reference beam. However, in some cases, a further correction of the Lap signal was performed by subtracting the absorption signal of a Lap film multiplied by a proportional factor.

Results and Discussion

For a common film thickness, an augmentation of the global color of the R6G/Lap films was observed by increasing the dye concentration and/or the immersion time.[34] Besides, the loading of the dye causes changes in the shape of the absorption spectra, for instance enhancing the absorption capacity of the dye at shorter wavelength as can be seen from the height-normalized absorption spectra shown in Figure 1. This change can be also analyzed by the decrease in the R parameter, defined as the ratio between the absorbance at the main band maximum (~528 nm) and that at the vibronic shoulder (~500 nm), $R \equiv A_{528}/A_{500}$.[34] The observed decrease in the R value by increasing the R6G loading suggests a metachromasy effect similar to that observed in liquid solutions.[35−37] This metachromasy is ascribed to the aggregation of the dye.[35−37,53]

For an adequate spectroscopic characterization of the dye aggregation, the recorded absorption spectra as a function of the R6G loading have to be normalized to a common dye concentration. Because it is difficult to know the exact concentration of dyes in the solid films (indeed, due to the low content of the organic material present in the film, CHN analysis of R6G/Lap films only provides an approximate value of the dye loading), the normalization factor cannot be exactly determined. Besides, the Beer law cannot be applied to a given wavelength because the dye aggregation affects the absorption capacity of the dye. To determine the concentration-normalized factor (σ), two approximate methods are proposed in the present paper:

- In the area-normalized method all the recorded spectra are normalized to the same area under the absorption curve of a reference sample, e.g., the most diluted R6G/Lap film. This method implies that the dye aggregation does not cause any hypo- or hyperchromic effect in the absorption band (the absorption ability of R6G molecules is independent of the aggregation state of the dye), as the exciton theory in zero-order approximation suggests. However, a slight hypochromic effect of 0.98 was experimentally observed for the aggregation of R6G in aqueous solution.[36]

- In the photometric method, the Beer law cannot be directly applied to a specific wavelength but to the average absorbance observed at the absorption maximum and the vibronic shoulder [$\bar{A} \equiv (A_{max} + A_{sh})/2$]. These two wavelengths were selected because the dye aggregation decreases/increases, respectively, the absorption probability at the monomeric band (~528 nm) and at the vibronic shoulder (~500 nm), as is indicated by the metachromasy effect. This method considers that the loss in the absorption capacity at the monomer band by the dye aggregation is compensated with the enhancement in the absorption probability of the aggregate at the vibronic shoulder. This method is only valid for a common thickness of the films, as is previously demonstrated for identical film preparation conditions.[34]

Therefore, the concentration-normalized σ factor is recounted for each sample by $\sigma = \text{area}/\text{area}_0$ (area method) or $\sigma = \bar{A}/\bar{A}_0$ (photometric method), where the subindex "0" refers to the corresponding parameter of the reference sample. Once the σ factor is known, the dye concentration (c) for each sample is referred to that of the reference sample (c_0) by $c = \sigma c_0$. The reference sample is considered that obtained by immersing the Lap film for 5 min into a 10^{-5} M solution of R6G, with a relative R6G/Lap concentration of around 0.1% CEC previously determined.[34]

The normalized absorption spectra obtained by both methods are shown in Figure 2. For moderate R6G loadings (from 0.1 to ~25% CEC, Figure 2a−h), both normalization methods give rise to an isosbestic point at ~508.5 nm (area method) or ~511.5 nm (photometric method). These isosbestic points confirm the validity of the present methods and the presence of a R6G aggregate species, considered in the first stage as a dimer. The disruption in the isosbestic point for further R6G loadings (>25% CEC, Figure 2i,j) would be attributed to the formation of high-order aggregates of the dye. In this case, the dye

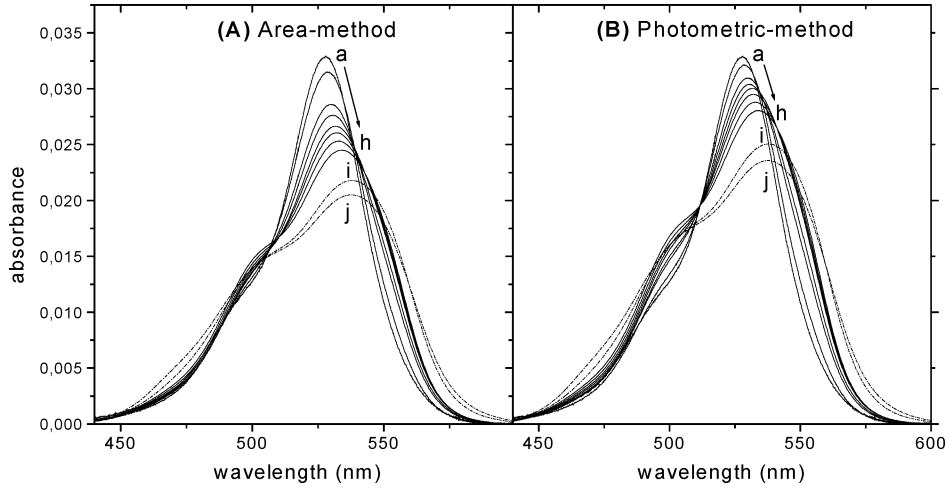

Figure 2. Evolution of the concentration-normalized absorption spectra of R6G intercalated in Lap films with the loadings (see Figure 1 caption): (A) area method and (B) photometric method.

aggregation also causes an increase in the absorption capacity of R6G at 470 nm.

The 3 nm discrepancy in the position of the isosbestic point between both normalization methods could be due to either an overestimation in the σ factor by the area method (probably due to a slight hypochromic effect by the dye aggregation) or an underestimation in this factor by the photometric method. (Indeed, as Figure 2 indicates, the decrease in the normalized absorbance at ~528 nm by the dye concentration is more extensive than the corresponding increase at ~500 nm.) Because the data provided by both methods give rise to similar interpretations, the normalized absorption spectrum for every sample is considered the average spectrum obtained by both normalization methods. In this case the obtained absorption spectra present an isosbestic point at 509.5 nm for moderate R6G loadings in Lap films (<25% CEC, data not shown).

Although the existence of the isosbestic point suggests the presence of only one type of R6G aggregate in equilibrium with the monomer, a qualitative analysis of the normalized spectra (Figure 2) also suggests that the dye aggregation enhances the absorption capacity of R6G at lower energies (higher wavelengths) with respect to the monomeric absorption band. This second absorption band of the aggregate does not generate a clear isosbestic point at around 535 nm, and the presence of a second R6G aggregate in moderate R6G loading samples (<25% CEC) cannot be ruled out. However, the existence of a high-order aggregate at these moderate loadings seems, from a spectroscopic point of view, to be very improbable because the ~509.5 nm isosbestic point would imply the same absorption coefficient for three R6G species (i.e., monomer, dimer, and trimer) at this wavelength. A more plausible explanation would be the evolution of the absorption bands of the R6G dimer with the dye concentration due to changes in the geometry of the aggregate with the R6G loading, as is discussed below.

To derive a quantitative procedure to evaluate the aggregation constant of R6G in Lap films, first, the formation of a dimer is considered in moderate R6G/Lap loadings (<25% CEC), i.e. in those R6G loadings included in the isosbestic point of Figure 2a−h. Defining the dimerization constant (K_D) as

$$M + M \underset{K_D}{\rightleftharpoons} D \qquad K_D = \frac{c_D/c^\circ}{(c_M/c^\circ)^2} \tag{1}$$

where c_M and c_D are the monomer (M) and dimer (D) concentrations in equilibrium, respectively, and c° is the standard concentration. If x is the molar fraction of the free monomer, then the equilibrium concentrations can be rewritten to the analytical concentration c by $c_M = cx$ and $c_D = c(1 - x)/2$. The analytical concentration of the sample is referred to the most diluted dye sample by the normalization factor ($c = \sigma c_0$). Therefore, the dimerization constant can be expressed by

$$K_D = \frac{1 - x}{2(c_0/c^\circ)\sigma x^2} \tag{2}$$

If the most diluted R6G/Lap film is considered as the standard ($c_o \equiv c^\circ$, for a real use of the σ factor, i.e., $\sigma = 1$ in the most diluted R6G/Lap film), the dimerization constant will be finally given by

$$K_D = \frac{1 - x}{2\sigma x^2} \tag{3}$$

So, K_D can be determined from the monomer molar fraction and the concentration factor (σ) for moderate dye loading samples. On the other hand, the x value can be evaluated from the normalized absorbance at any wavelength by applying the Beer−Lambert law:

$$\frac{A(\lambda)}{\sigma} = \epsilon_M(\lambda)c_0 x l + \epsilon_D(\lambda)c_0(1 - x)l = A_M(\lambda)x + A_D(\lambda)(1 - x) \tag{4}$$

where $\epsilon_M(\lambda)$ and $\epsilon_D(\lambda)$ represent the molar absorption of the monomer and of the monomer units in the dimer at the wavelength λ, respectively, and l is the thickness of the films. The $A_M(\lambda) = \epsilon_M(\lambda)c_0 l$ and $A_D(\lambda) = \epsilon_D(\lambda)c_0 l$ terms represent the absorbance of the monomer and of the monomer units in the dimer, respectively, referred to the reference concentration c_0 and the films thickness l.

The absorption spectrum of the R6G monomer in the Lap film can be matched to that recorded for the most diluted sample, used as reference (Figure 2a). It is experimentally confirmed that the shape of this absorption spectrum does not change for further R6G dilutions, ruling out the presence of any R6G aggregates affecting the absorption band. Moreover, the shape of this absorption spectrum, with an $R \equiv A_{max}/A_{sh} = 2.9$ parameter, is similar to that obtained for the R6G monomer in liquid water ($R = 2.7$) and ethanol ($R = 3.3$). However, a general wider absorption band is obtained in the solid sample, which

could be attributed to an electronic interaction between the aromatic π-system of the dye and the electron lone pair of the surface O atoms of the clay (although a certain degree of dye aggregation, undetectable by absorption spectroscopy, cannot be ruled our for this sample because its fluorescence decay curve cannot be analyzed as a monoexponential decay;[52] data not shown). We have considered this 0.1% CEC sample as the diluted reference sample because further decrease in the dye loadings leads to an important decrease in the signal-to-noise ratio due to the very low absorbance of these samples ($A_{max} < 0.02$).

The subtraction of the contribution of the monomer absorption from the recorded spectra (eq 4) cannot be realized because the molar fraction of the monomer in equilibrium with the dimer is not known, and the pure absorption spectrum of the dimer cannot be experimentally recorded. Therefore, different mathematical procedures have been developed to obtain the aggregation constant and the pure absorption spectrum of the aggregates.

An approximate method is based on the evolution of the $R \equiv A_{max}/A_{sh}$ parameter with the dye concentration.[54] In a first approximation the x value ($x^{(1)}$) is determined from the R/R_0 ratio, where R_0 is the corresponding R parameter for the monomer absorption spectrum, that for the reference sample (Figure 2a). This assumption is valid when the absorption capacity of the dimer ($\epsilon_D(\lambda)$) at λ_{max} and λ_{sh} is much lower and similar, respectively, with respect to that of the monomer ($\epsilon_M(\lambda)$), i.e. $\epsilon_D(\lambda_{max}) \ll \epsilon_M(\lambda_{max})$ and $\epsilon_D(\lambda_{sh}) \approx \epsilon_M(\lambda_{sh})$. This initial $x^{(1)}$ provides an approximate dimerization constant $K_D^{(1)}$ and absorption spectrum of the dimer $\epsilon_D^{(1)}(\lambda)$ for each dye concentration, and average $\bar{K}_D^{(1)}$ and $\bar{\epsilon}_D^{(1)}(\lambda)$ values can be obtained from all considered dye concentrations. From this $\bar{K}_D^{(1)}$ value, a more precise molar fraction $x^{(2)}$ can be evaluated for every dye concentration. The procedure is repeated by an iterative process to reach an accurate $x^{(n)}$ value. This method is suitable for sandwich dimers in which the aggregation bears important losses in the intensity of the main monomer absorption band (i.e., $\epsilon_D(\lambda_{max}) \ll \epsilon_M(\lambda_{max})$).[35−37] However, considering the evolution of the absorption spectra of R6G/Lap system shown in Figure 2, this iterative method cannot provide successful results. Indeed, it has been confirmed by computer simulations that this iterative method overestimates the K_D value for dimers with the long-wavelength absorption band more intense than the monomer band (head-to-tail dimer). The advantage of this method is the estimation of an approximate molar fraction of the monomer without the knowledge of the analytical concentration of the dye.

An alternative and more precise method to evaluate dimerization constant, K_D, and the dimer absorption spectrum, $\epsilon_D(\lambda)$, is by means of a nonlinear least-squares method in which the best K_D and $\epsilon_D(\lambda)$ values are adjusted to explain the evolution of the absorption spectra with the dye concentration. Taking the x value from the eq 3 and inserting it in eq 4, the following expression can be drawn out:

$$\frac{A(\lambda)}{\sigma} = [\epsilon_M(\lambda) - \epsilon_D(\lambda)]c_0 l \frac{\sqrt{1 + 8K_D\sigma} - 1}{4K_D\sigma} + \epsilon_D(\lambda)c_0 l \quad (5)$$

Hence, the evolution of the normalized absorbance ($A(\lambda)/\sigma$) vs the concentration factor (σ) would give us the dimerization constant (K_D) and the absorption spectrum of the dimer ($\epsilon_D(\lambda)$).

The nonlinear fit, performed by the ORIGIN 6.1 software, is based on the Levenberg−Marquardt algorithm.[55] The fit provides those K_D and $\epsilon_D(\lambda)$ values that minimize the reduced chi-square between the experimental and the fitted data. Figure 3 shows the fit curve obtained for the R6G/Lap film in moderate dye loadings at the three most representative wavelengths: the main absorption band of the monomer (528 nm) and around the absorption wavelength of H- and J-band of the dimer (500 and 545 nm), although the fit could be extrapolated to any wavelength in the absorption range. The fit was realized as a global analysis at the three wavelengths: $\epsilon_D(\lambda_i)$ are independent adjustable parameters whereas K_D is an adjustable parameter but linked to be a common value to all the analysis wavelengths. In the fitting procedure the $\epsilon_M(\lambda_i)$ can be considered as fixed (i.e., the experimental absorption spectrum of the monomer, Figure 2a) or as adjusted parameters obtained for the $A(\lambda_i)/\sigma$ value extrapolated to infinite dilution, $\sigma \rightarrow 0$. In this last case, the experimental data obtained for the reference sample are included in the fitting with a very small σ value (around 0.1). This last procedure provides similar $\epsilon_M(\lambda_i)$ values to those experimentally observed. Both fits supply analogous values with correlation coefficients (r) close to unity, suggesting the viability of the mathematical procedure.

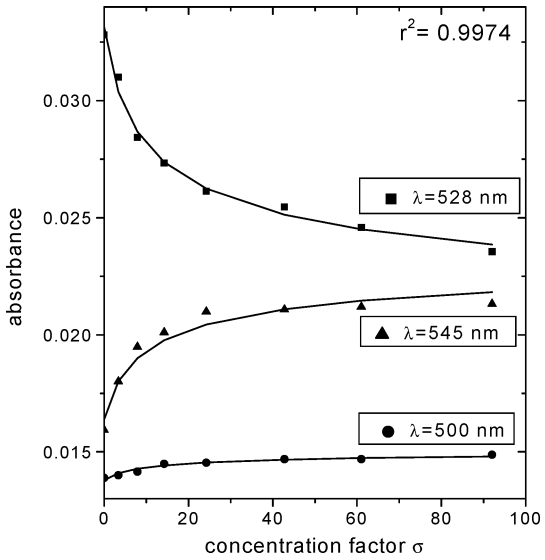

Figure 3. Global nonlinear curve fit of eq 5 at three representative wavelengths. The global correlation coefficient is inset.

The global analysis proposes a K_D value of 0.043 (standard concentration, $c^o \equiv$ 0.1% CEC R6G/Lap film) for the dimer characterized for moderate R6G loading samples (from 1 to ∼25% CEC), from which, and applying eq 3 and eq 4, an absorption spectrum for the dimer can be obtained for every sample, some of which are shown in Figure 4. These spectra consist of two absorption bands placed at both sides of the monomer absorption band, which is consistent with the exciton theory for twisted sandwich type (case D_1 in Scheme 1) or oblique head-to-tail type (case D_2, Scheme 1) dimers.[40,41] Taking into account that the J-band (centered at lower energies) is around 1.5 more intense than the H-band, a head-to-tail geometry can be characterized for the R6G dimer in the interlayer space of Lap films.[43]

A more precise analysis of the calculated absorption spectrum of the dimer indicates that the shape of this spectrum is not actually independent of the dye concentration in the moderate loading range of 1−25% CEC, but rather the absorption capacity of the H-band increases in detriment of the J-band as the R6G loading increases (Figure 4). These evolutions with the dye loadings could be assigned to several factors:

- The progressive formation of a new aggregate. Indeed, the coexistence of H-dimers and J-dimers of rhodamines in different

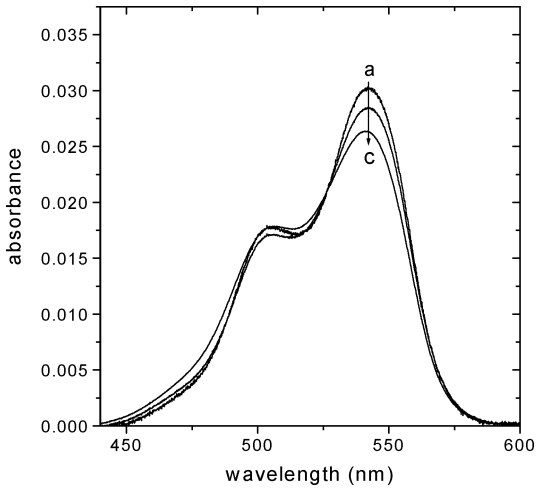

Figure 4. Calculated absorption spectrum of the R6G dimer obtained at three moderate dye concentrations (% CEC): 2.0 (a), 5.7 (b), and 21 (c).

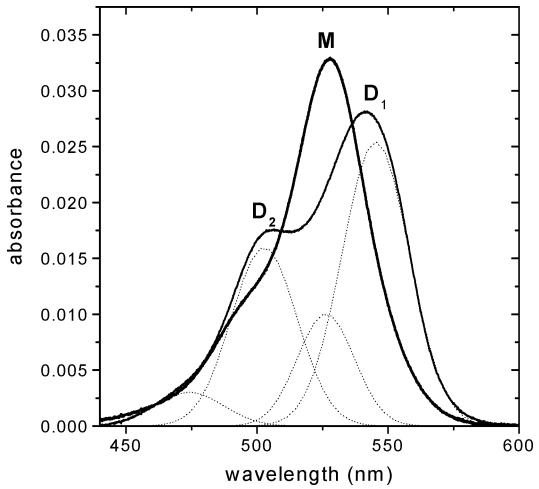

Figure 5. Average absorption spectrum (solid line) of the R6G dimer in Lap films obtained in moderate dye loadings (from 1 to 21% CEC). The splitting in four Gaussian curves (dashed lines) and the monomer absorption spectrum are also included.

interfaces and surfaces has been proposed by several authors.[56,57] Moreover, the shape of the absorption spectrum of the dimer calculated for the 21% CEC sample (Figure 4c), with an incipient absorbance at 470 nm, could indicate the presence of a small proportion of a higher-order aggregate (trimer or so on).

- The geometry of the dimer evolves with the dye loading. Some authors[17,58,59] have proposed that R6G molecules are disposed more perpendicular with respect to the clay surface as the loading of the dye is increased. Such a different disposition of the monomeric units would affect the geometry of the dimer and consequently affect the shape of its absorption spectrum. Indeed, a more perpendicular disposition of the monomeric units would decrease the torsion angle α of the head-to-tail dimer, and consequently the intensity of both absorption bands of the dimer would tend to be equal, as Figure 4 suggests. This evolution in the dimer geometry could be consistent with the isosbestic point at around 510 nm.

- Finally, the presence of the organic dye would decrease the polarity in the interlayer space of the Lap films with the loading, affecting the position of the monomeric absorption band.[38,60] Consequently, $\epsilon_M(\lambda_i)$ cannot be considered as an adjustable parameter in eq 5, but as a dye loading-dependent variable. This effect would shift both the absorption and the fluorescent band of the dye to a similar extent.[60] However, this phenomenon can be ruled out in the present system because the displacement of the fluorescence band (around 40 nm,[52] data not shown) is much more important than that observed in the absorption spectra (around 10 nm, Figure 2).

To apply the exciton theory and to obtain a general information on the geometry parameters of the dimer, an average absorption spectrum of the dimer is considered for moderate R6G loadings (<25% CEC) (Figure 5). The deconvolution of this absorption spectrum in several Gaussian curves (by means of the Origin 6.1 software) allows us an adequate characterization of the absorption parameters, which are summarized in Table 1. Thus, the two main absorption bands of the dimer, localized at $\lambda_1 \approx 545$ nm and $\lambda_2 \approx 504$ nm, have associated a respective second low-intense Gaussian curve placed at higher energies. These low-intense Gaussians can be ascribed to the corresponding vibronic transition of the two main Gaussians, similar to the absorption shoulder associated with the main absorption band of the monomer. The area under the curve of both absorption bands of the dimer is $f_1 = 0.484$ and $f_2 = 0.308$ for the higher and lower energies bands, respectively (Table 1). From these spectroscopic characteristics, the geometry parameters (intermolecular distance, R, and angle between the dipole moment, α, between the monomeric units) of the dimer can be obtained from the interaction energy between the monomeric units in the dimer (U), the ratio of the oscillator strength of both dimer absorption bands (f_1/f_2), and the oscillator strength of the monomeric band (f_M) by means of the following equations derived from the exciton theory:[40,41,61]

$$U = \frac{\nu_2 - \nu_1}{2} \tag{6}$$

$$\tan^2(\alpha/2) = \frac{f_1 \nu_2}{f_2 \nu_1} \tag{7}$$

$$R^3 = \frac{2.14 \times 10^{10}[\cos\alpha + 3\,\mathrm{sen}^2(\alpha/2)] f_M}{\nu_M (2U)} \tag{8}$$

where the wavenumber (ν) is expressed in cm^{-1} and R in Å. Because the absolute dye concentration and optical pathway values of the reference sample are not known, the f_M value cannot be determined from the area under the curve of the monomer absorption band (Figure 2a). If the absorption capacity of R6G monomer in the film is similar to that in liquid solutions, then the f_M value can be estimated from the absorption spectrum of a diluted solution of R6G ($f_M = 0.71$ in ethanol). Applying eqs 6−8 to the above results, an oblique head-to-tail dimer with a intermolecular distance of 9.5 Å and a torsional angle of 105° is characterized for the R6G aggregate in Lap films in moderate dye loadings (<25% CEC) (Table 1). Similar geometry parameters ($R \approx 9.5$ Å and $\alpha \approx 109°$, Table 1) are obtained from the absorption spectrum of the dimer obtained for the lowest dye loading film (2% CEC). These results suggest that changes in the absorption spectrum of the dimer with the loading in the <25% CEC range (Figure 4) do not appreciably affect the geometry of the aggregates, although a slightly more aligned head-to-tail dimer in low dye loading samples cannot be excluded. This conclusion would agree with a more perpendicular disposition of the rhodamine molecules in the clay surface by increasing the dye loading.[17,58,59]

This dimer contracts with the sandwich-type R6G dimer previously characterized in the interlayer space of Lap particles in aqueous suspensions.[62] In this case, and due to the high

TABLE 1: Spectroscopic (Absorption Maxima and Oscillator Strength) and Geometric (Intermonomeric Distance and Torsional Angle) Parameters of the Oblique Head-to-Tail Dimer of R6G Absorbed in Solid Thin Films of Lap Characterized for Moderate Dye Loadings (1−25% CEC); Spectroscopic Properties of the Monomer Are Also Included

	spectroscopic parameters		
monomer (0.1% CEC)	$\lambda_M = 527.9$ nm	$\nu_M = 18943$ cm^{-1}	$f_M = 0.710^a$
dimer (average: 1−25% CEC, Figure 5)	$\lambda_1 = 544.9$ nm	$\nu_1 = 18352$ cm^{-1}	$f_1 = 0.484^a$
	$\lambda_2 = 503.7$ nm	$\nu_2 = 19853$ cm^{-1}	$f_2 = 0.308^a$
dimer (2% CEC, Figure 4a)	$\lambda_1 = 546.0$ nm	$\nu_1 = 18315$ cm^{-1}	$f_1 = 0.522^a$
	$\lambda_2 = 502.9$ nm	$\nu_2 = 19885$ cm^{-1}	$f_2 = 0.282^a$
	geometric parameters		
dimer (average: 1−25% CEC, Figure 5)	$U = 750$ cm^{-1}	$R = 9.54$ Å	$\alpha = 105°$
dimer (2% CEC, Figure 4a)	$U = 785$ cm^{-1}	$R = 9.48$ Å	$\alpha = 109°$

[a] On the basis of the integrated absorption band of the 0.1% CEC sample and normalized to the value obtained in ethanol.

wettability character of the Lap tactoids, the interlayer distance can be modified to any value to accommodate the most stable R6G dimer, e.g., a sandwich-type aggregate. However, in solid films, the interlayer space is more constrained, and the geometry of the formed dimer is imposed by this limitation, leading to a head-to-tail dimer structure. On the other hand, and due to the hydrophobicity of the dye, rhodamine 3B forms head-to-tail dimers in the interlayer space of Lap tactoids in aqueous suspension. In that case an intermonomeric torsional angle of 82° was reported,[63] lower than the present case. In liquid suspension, and due to the swelling properties of the Lap interlayer space, a more oblique head-to-tail dimer is possible whereas in solid films, and because of their rigidity, the twisted angle of the dimer is governed by the interlayer distance.

For high loading samples (>25% CEC), a high-order aggregate should be formed because of the disruption of the isosbestic point (Figure 1). This high-order aggregate would be characterized, besides other parameters, by an absorption band centered at around 470 nm, which is consistent with the exciton theory, which proposes an absorption band at higher energies for such a kind of molecular association. This absorption characteristic is similar to that reported for the high-order aggregate of rhodamine 3B in aqueous suspensions of Laponite, where a head-to-tail dimer was also characterized.[46] In this case and due to the geometric disposition of the monomer units in head-to-tail aggregates, the interlayer space of clay tactoids is not a limitation to incorporate new monomer units to get high-order head-to-tail aggregates. This is not the case for a sandwich dimer (for instance, for the aggregation of R6G in clay particles in aqueous suspensions[45,62,63]) where the restraint of the interlayer space for a third monomer unit prevented the formation of high-order aggregates for a parallel disposition of the aromatic ring into the clay layer.

The head-to-tail nature of the R6G aggregates in Lap films can be confirmed by fluorescence data, which will be discussed in an additional paper.[52]

Conclusions

Several mathematical procedures have been designed to evaluate the aggregation constant and the absorption spectrum of the dimer of dyes incorporated in solid samples. First, the dye concentration has to be referred to a reference sample, for instance the most diluted one, from which a concentration factor is obtained. Then, the evolution of the concentration-normalized absorption spectra with the dye loading (or the concentration factor) is fitted to a nonlinear curve based on the law-mass and the Beer−Lambert laws, from which the best adjustable dimerization constant and absorption spectrum parameters (those minimizing the chi-square statistical parameter between the experimental and the theoretical data) for the aggregate are obtained. This curve fitting can be realized in all the absorption range or at those most representative wavelengths by a global analysis. The calculated absorption spectrum of the R6G dimer adsorbed in the interlayer space of Lap films for moderate dye loadings (from 1 to 25% CEC) reveals a head-to-tail dimer with an intermonomeric distance of ∼9.5 Å and an angle of ∼105° between the dipole moment of the monomer units. This aggregate contrasts with the sandwich-type dimer of R6G observed in the interlayer space of Lap tactoid in aqueous suspensions, probably because the limitation of the interlayer distance in solid films prevents the pile-up of two parallel xanthene planes to the clay surface to form the rhodamine dimer. Further increases in the dye loading (>25% CEC) give rise to higher-order aggregates, characterized at least by an absorption band at 470 nm.

Acknowledgment. This work is supported by the University of the Basque Country UPV/EHU (research project: 9/UPV-00039.310-15264/2003). V.M.M. and J.B.P. thank the Spanish MECyD Minister and the UPV-EHU, respectively, for research grants.

References and Notes

(1) Ye, C.; Lam, K. S.; Chik, K. P.; Lo, D.; Wong, K. H. *Appl. Phys. Lett.* **1996**, *69*, 3800−3802.
(2) Wu, S.; Zhu, C. *Opt. Mater.* **1999**, *12*, 99−103.
(3) Schulz-Ekloff, G.; Wöhrle, D.; Van Duffel, B.; Schoonheydt, R. A. *Microporous Mesoporous Mater.* **2002**, *51*, 91−138 and references therein.
(4) Sasai, R.; Ogiso, H.; Shindachi, I.; Shichi, T.; Takagi, K. *Tetrahedron* **2000**, *56*, 6979−6984.
(5) Sasai, R.; Itoh, H.; Shindachi, I.; Shichi, T.; Takagi, K. *Chem. Mater.* **2001**, *13*, 2012−2016.
(6) Jones, R. M.; Lu, L.; Helgeson, R.; Bergstedt, T. S.; McBranch, D. W.; Whitten, D. G. *Proc. Natl. Acad. Sci. U.S.A.* **2001**, *98*, 14769−14772.
(7) Mitzi, D. B. *Chem. Mater.* **2001**, *13*, 3283−3298.
(8) Carotenuto, G.; Her, Y. S.; Matijevic, E. *Ind. Eng. Chem. Res.* **1996**, *35*, 2929−2932.
(9) Calzaferri, G.; Huber, S.; Maas, H.; Minkowski, C. *Angew. Chem., Int. Ed.* **2002**, *42*, 3732−3758.
(10) Schoonheydt, R. A. *Clays Clay Miner.* **2002**, *50*, 411−420.
(11) Ogawa, M.; Kuruda, K. *Chem. Rev.* **1995**, *95*, 399−438.
(12) Ramamurthy, V., Ed. *Photochemistry in Organized and Constrain Media*; VCH: New York, 1991.
(13) Thomas, J. K. *Chem. Rev.* **1993**, *93*, 301−320.
(14) Ramamurthy, V.; Eaton, D. F. *Chem. Mater.* **1994**, *6*, 1128−1136.
(15) Van Duffel, B.; Verbiest, T.; Van Elshocht, S.; Persoons, A.; De Schryver, F. C.; Schoonheydt, R. A. *Langmuir* **2002**, *17*, 1243−1249.
(16) Miyamoto, N.; Kawai, R.; Kuruda, K.; Ogawa, M. *Appl. Clay Sci.* **2001**, *19*, 39−46.
(17) Iyi, N.; Kurashima, K.; Fujita, T. *Chem. Mater.* **2002**, *14*, 583−589.
(18) Sonobe, K.; Kikuta, K.; Takagi, K. *Chem. Mater.* **1999**, *11*, 1089−1093.
(19) Hussein, B. M. Z.; Zainal, Z.; Yahaya, A. H.;. Asís, A. B. A. *Mater. Sci. Eng.* **2002**, *B88*, 98−102.
(20) Ray, K.; Nakahara, H. *J. Phys. Chem. B* **2002**, *106*, 92−100.

(21) Hagerman, M. E.; Salamone, S. J.; Herbst, R. W.; Payeur, A. L. *Chem. Mater.* **2003**, *15*, 443−450.
(22) Giannelis, E. P. *Chem. Mater.* **1990**, *2*, 627−629.
(23) Shichi, T.; Takagi, K. *J. Synth. Org. Chem. Jpn.* **2002**, *60*, 1076−1086.
(24) Ogawa, M.; Kuruda, K. *Bull. Chem. Soc. Jpn.* **1997**, *70*, 2593−2618.
(25) Miyamoto, N.; Kuroda, K.; Ogawa, M. *J. Mater. Chem.* **2004**, *14*, 165−170.
(26) Place, I.; Penner, T. L.; McBranch, D. W.; Whitten, D. G. *J. Phys. Chem. A* **2003**, *107*, 3169−3177.
(27) Takenawa, R.; Komori, Y.; Hayashi, S.; Kawamata, J.; Kuroda, K. *Chem. Mater.* **2001**, *13*, 3741−3746.
(28) Umemura, Y.; Yamagishi, A.; Schoonheydt, R.; Persoons, A.; De Schryver, F. C. *J. Am. Chem. Soc.* **2002**, *124*, 992−997.
(29) Drexhage, K. M. In *Dye Laser;* Schäfer, F. P., Ed.; Springer-Verlag: Berlin, 1990; Vol. 1.
(30) Newmann, A. C. D. *Chemistry of Clays and Clay Minerals*; Longman Science Technology Mineral Society: London, 1987.
(31) Van Olphen, H. *An Introduction to Clay Colloid Chemistry*; Wiley: New York, 1977.
(32) Odom, I. E. *Philos. Trans. R. Soc. London A* **1984**, *311*, 391−409.
(33) Newman, S. P.; Jones, W. *New J. Chem.* **1998**, 105−115.
(34) Martínez, V.; López Arbeloa, F.; Bañuelos, J.; Arbeloa López, T.; López Arbeloa, I. *Langmuir* **2004**, *20*, 5709−5717.
(35) López Arbeloa, F.; Llona González, I.; Ruiz Ojeda, P.; López Arbeloa, I. *J. Chem. Soc., Faraday Trans. 2* **1982**, *78*, 989−994.
(36) López Arbeloa, F.; Ruiz Ojeda, P.; López Arbeloa, I. *J. Chem. Soc., Faraday Trans. 2* **1988**, *84*, 1903−1912.
(37) Rohatgi-Mukherjee, K. K. *Indian J. Chem.* **1992**, *31A*, 500−511.
(38) Van der Auweraer, M.; Verschuere, B.; De Schryver, F. C. *Langmuir* **1998**, *4*, 583−588.
(39) Tsukanova, V.; Lavoie, H.; Harata, A.; Ogawa, T.; Salesse, C. *J. Phys. Chem. B* **2002**, *106*, 4203−4213.
(40) McRae, E. G.; Kasha, M. *Physical Process in Radiation Biology;* Academy Press: New York, 1964.
(41) Kasha, M.; Rawls, H. R.; El-Bayoumi, M. A. *Pure Appl. Chem.* **1965**, *11*, 371−392.
(42) Antonov, L.; Gergov, G.; Petrov, v.; Cubista, M.; Nygren, J. *Talanta* **1999**, *49*, 99−106.
(43) Fujii, T.; Nishikiori, H.; Tamura, T. *Chem. Phys. Lett.* **1995**, *233*, 424−429.
(44) Ballet, P.; Van der Auweraer, M.; De Schryver, F. C. *J. Phys. Chem.* **1996**, *100*, 13701−13715.
(45) López Arbeloa, F.; López Arbeloa, T.; López Arbeloa, I. *Trends Chem. Phys.* **1996**, *4*, 191−213.
(46) López Arbeloa, F.; Martínez, V.; Bañuelos, J.; López Arbeloa, I. *Langmuir* **2002**, *18*, 2658−2664.
(47) Bujdák, J.; Nobou, I. *Clays Clay Miner.* **2002**, *50*, 446−454.
(48) Bujdák, J.; Nobou, I.; Hrobáriková, J.; Fujita, T. *J. Colloid Interface Sci.* **2002**, *247*, 494−503.
(49) Yariv, S. *Int. J. Trop. Agric.* **1988**, *VI*, 1−19.
(50) Shichi, T.; Takagi, K. *J. Photochem. Photobiol. C* **2000**, *1*, 113−130.
(51) Van Olphen, H.; Fripiat, J. J. *Data Handbook for Clay Minerals and other Non-Metallic Minerals*; Pergamon Press: London, 1979.
(52) Martínez Martínez, V.; López Arbeloa, F.; Bañuelos Prieto, J.; Arbeloa López, T.; López Arbeloa, I., to be submitted.
(53) Cenens, J.; Schoonheydt, R. A. *Clays Clay Miner.* **1988**, *36*, 214−224.
(54) López Arbeloa, I. *J. Chem. Soc., Faraday Trans. 2* **1982**, *77*, 1725−1734.
(55) Marquardt, W. *J. Soc. Indust. Appl. Math.* **1963**, *11*, 431.
(56) Nishikiori, H.; Fujii, T. *J. Phys. Chem. B* **1997**, *101*, 3680−3687.
(57) del Monte, F.; Levy, D. *J. Phys. Chem. B* **1999**, *103*, 8080−8086.
(58) Endo, T.; Nakada, N.; Sato, T.; Shimada, M. *J. Phys. Chem. Solids* **1989**, *50*, 133−137.
(59) Iwasaki, M.; Kita, M.; Ito, K.; Cono, A.; Fukunishi, K. *Clays Clay Miner.* **2000**, *48*, 392−399.
(60) Pevenage, D.; Van der Auweraer, M.; De Schryver, F. C. *Langmuir* **1999**, *15*, 8465−8473.
(61) Vuorimaa, E.; Ikonen, M.; Lemmetyinen, H. *Chem. Phys.* **1994**, *188*, 298−302.
(62) Tapia Estévez, M. J.; López Arbeloa, F.; López Arbeloa, T.; López Arbeloa, I. *J. Colloid Interface Sci.* **1994**, *162*, 412−417.
(63) López Arbeloa, F.; Herrán Martínez, J. M.; López Arbeloa, T.; López Arbeloa, I. *Langmuir* **1998**, *14*, 4566−4573.